Mon. Not. R. Astron. Soc. **317**, 391–405 (2000)

Modelling near-IR spectra and mid-IR dust emission of Mira variables at different phases

A. Lobel,[1★] S. Bagnulo,[2] J. G. Doyle[3] and C. Power[3]
[1]*Harvard-Smithsonian Center for Astrophysics, 60 Garden Street, Cambridge, MA 02138, USA*
[2]*Institut für Astronomie, Universität Wien, Türkenschanzstrasse 17, A-1180 Wien, Austria*
[3]*Armagh Observatory, College Hill, Armagh BT61 9DG*

Accepted 2000 March 23. Received 2000 February 25; in original form 1999 November 11

ABSTRACT

We model the spectral changes of late oxygen-rich Miras observed in different pulsation phases. From a combination of variable near-IR spectra and UKIRT spectro-photometry of the 9.7-μm silicate dust emission feature in different phases we study the influence of the changing atmospheric circumstances on the conditions in the circumstellar dust shell. From a detailed modelling of TiO and VO bands in the near-IR spectra, we determine changes of the effective temperature and the effective atmospheric acceleration of the central star. The corresponding model spectral energy distribution is redistributed through the dust shell by means of radiative transfer calculations in order to perform a detailed modelling of shape changes observed in the silicate feature. We show that the latter are mainly caused by changes in the flux distribution of the incident radiation field with stellar pulsation, whereas intensity changes of the dust emission result from stellar luminosity changes as they are enshrouded by very optically thin dust shells. In the case of the Mira *o* Cet we compute that the effective temperature increases from $T_{\rm eff} = 2400\,{\rm K}$ in the minimum phase to 3000 K ($\pm 100\,{\rm K}$) around the maximum phase. The amplified momentum transfer around maximum light enhances the acceleration of the dust outflow near the dust condensation radius of $\sim 6\,R_*$. This produces variations of the terminal dust outflow velocity with phase ($\Delta v_\infty \simeq 5\,{\rm km\,s^{-1}}$) at larger distance from the star. The corresponding small changes in flux mean opacity and gas mass-loss rates (from 2.8 to $3.2 \times 10^{-7}\,{\rm M_\odot\,yr^{-1}}$) are sufficient to model the shape changes observed in the dust emission feature. A comparison with the modelling results for another long period Mira, U Ori, is also provided.

Key words: stars: AGB and post-AGB – circumstellar matter – stars: individual: *o* Cet – stars: individual: U Ori – stars: variables: other – infrared: stars.

1 INTRODUCTION

In this paper we analyse the near-IR spectra of two oxygen-rich luminosity class III giants having regular light-curves of the Mira Ceti type. These 'Mira variables' are commonly termed as 'slow' pulsators, with long periods (LPV) ranging from 150 to 500 d. Their visual continuum radiation is strongly attenuated by water vapour and metaloxides like titanium oxide (TiO) and vanadium oxide (VO). In the latest-M Miras, bands of VO are more suitable than TiO for a refined determination of small changes in the atmospheric conditions with phase. Such prominent changes in the strength and shape of the VO bands have already been observed by Miller (1956) in S Umi. We study the effects of pulsation on the atmospheric model parameters of two late-M-type Miras, *o* Cet and U Ori, by modelling the VO band at 7450 Å. These near-IR spectra were observed by Castelaz & Luttermoser (1997) in different variability phases, with signal-to-noise ratios and a spectral resolution (1.08 Å per pixel), which is sufficient to allow a comparison with detailed synthetic model spectra for low-$T_{\rm eff}$ M-S-C giants, released by Allard et al. (1995).

The presence of dust shells around these very cool and luminous objects offers an important opportunity to study the effects of atmospheric oscillations on the circumstellar environment. Creech-Eakman et al. (1997) observed variations of the mid-IR silicate feature of LPVs and hypothesized that it may result from changing local thermodynamic conditions of the dust by an impinging circumstellar shock wave. The two phases were however observed nearly a decade apart. In a study of two *IRAS* LRS spectra taken at different phases of the Mira AU Cyg, Little-Marenin, Stencel & Staley (1996) suggested changes in the grain size distribution by the evaporation of larger grains towards maximum light. Only recently Monnier, Geballe & Danchi (1998)

★ E-mail: alobel@cfa.harvard.edu

have collected a homogeneous set of mid-IR UKIRT spectrophotometry results in the same or subsequent pulsation phases. They observed a significant sharpening of the 9.7-μm dust emission feature near the visual maximum for objects with optically thin dust shells like IK Tau, *o* Cet and U Ori and conjectured possible changes in the dust emissivity or optical properties by dust heating and cooling effects during a cycle (see also Le Bertre 1993).

In this paper we model the shape changes of the silicate emission spectra of these two Miras provided by Monnier et al. (1998). We perform radiative transfer calculations in different phases with the DUSTY code (Ivezić, Nenkova & Elitzur 1996), which can incorporate the atmospheric model spectra selected by observed near-IR spectra for the corresponding variability phases. This unique combination of spectral data and theoretical modelling enables us to test possible interaction mechanisms between the variable stellar radiation field and conditions in the circumstellar environment of late-M Miras and to constrain related properties of dust and gas outflow. We will show, for instance, that the observed shape changes of the mid-IR emission feature can be explained as a dynamic response of the circumstellar dust shell (CDS) to the stellar flux variations, without invoking changes in the dust properties.

The paper is organized as follows. In Section 2 we discuss properties of the input atmospheric model grid. We discuss the sensitivity of the VO band at 7334 Å and compare model spectra from different spectral synthesis codes. In Section 3 we develop a least squares method to fit the observed near-IR spectra. A brief description of the radiative transport calculations in the CDS to model variable silicate features is also provided. The results of application of both modelling methods to the observed near-IR and mid-IR spectra of [o Cet and U Ori] are given in Section 4, together with a discussion of the consequences for pulsation on the conditions in the CDS. The conclusions of this modelling work are summarized in Section 5.

2 SPECTRAL MODEL GRID

The stellar synthetic spectra were computed by Allard et al. (1995) (for a description of the equation of state and the radiative transfer in spherical geometry and hydrostatic equilibrium with the PHOENIX code, we refer the reader to Allard & Hauschildt 1995). These model spectra include opacities from important diatomic (and polyatomic) absorbers like CN, OH, CO, TiO, SiO, FeO, ZrO and VO. Convection is included in the mixing length approximation with $l/H = 1.0$. The resolution of the models up to 2.5 μm is 2 Å, which is sufficient to compare with the observed resolution and to model the detailed shape of broad molecular bands. The grid is provided for $2200\,\mathrm{K} \leqslant T_{\rm eff} \leqslant 4000\,\mathrm{K}$, $-1.0 \leqslant \log(g) \leqslant 0.5$ and $0.27 \leqslant \mathrm{C/O} \leqslant 1.02$ (by number) for $L_* = 10\,000\,\mathrm{L}_\odot$. Note that for solar abundance ($\mathrm{C/O} = 0.4401$) and solar metallicity, the grid is available in steps of $\Delta T_{\rm eff} = 100\,\mathrm{K}$ and $\Delta\log(g) = 0.5$, which is required for the refined and automated search technique described below.

2.1 Temperature and gravity dependence

In Fig. 1(a) we show a high-resolution spectral model with $T_{\rm eff} = 2700\,\mathrm{K}$, $\log(g) = -1.0$ and $L_* = 10\,000\,\mathrm{L}_\odot$, for solar abundance. For display purposes we have smoothed the models with a Gaussian filter in order to view the broad molecular bands and to define a local mean level (white lines). The flux for a 2700 K blackbody is shown as a dotted line. Intense molecular absorption bands appear below 1 μm. Continuum radiation emerges at the base of the atmosphere beyond optical depths of $\log(\tau) = 1$. In the near- and mid-IR, the atmospheric fluxes exceed the blackbody fluxes as optical energy is redistributed there and the bolometric flux must remain conserved. Fig. 1(b) shows that the flux increase becomes particularly strong around 1.7 μm (the *H* passband) as the effective gravity is increased from −1.5 or −1.0 (bold line) to −0.5 (thin line) and 0.0 (dash–dotted line), keeping all other model parameters fixed. The scatter in colour for different gravity values amplifies towards lower $T_{\rm eff}$ as the atmospheric extension increases. Beyond 3 μm the model continua quickly converge, nearly assuming the Planckian distribution and flux levels. In low-mass, high-luminosity late M-type giants, the gas pressure scale height ($H_{\rm p}$) around $\tau = 1$ becomes proportional to the stellar radius, leading to geometrically extended photospheres owing to small ratios of the effective and Newtonian gravity. Therefore, opacities react sensitively to the resulting geometrical and molecular cooling (especially for H_2O line opacity) owing to the dilution and peaking of radiation (Allard, Scholz & Wehrse 1992).

As the effective acceleration is a locally defined quantity $g_{\rm eff} = -1/\rho(\mathrm{d}P/\mathrm{d}r)$, an increase of $g_{\rm eff}$ may be caused by an increase of the photospheric pressure gradient and decrease of $H_{\rm p}$, but also by an increase of the gas density and pressure at comparable optical depths (for atmospheric model structures of different gravity see i.e. Plez 1992). Such changes of local thermodynamic quantities with geometrical extension affect the local excitation fraction of molecules like TiO and VO (with rather low binding energies of 6–7 eV), formed in outer layers. The local excitation temperature and equilibrium dissociation fractions determine the line intensities of their electronic transitions. In Fig. 1(c) one observes at 0.75 μm how the VO band of the *B*–*X* system (a $\Delta v = 1$ transition with bandhead at 7334 Å) strengthens with increasing gravity, keeping $T_{\rm eff}$ fixed. This is because the kinetic temperature, together with the partial pressures, in the outermost layers (where $T_{\rm kin} \leqslant 1900\,\mathrm{K}$ for $\log(\tau_{\rm Ross}) \leqslant -4$) slightly but appreciably increases by about 200 K at these low gravity values. The sensitivity of this low excitation band with respect to the neighbouring TiO bands (γ-system with transitions R_3 0-0 at 7054 Å and R_3 0–1 at 7589 Å) renders it therefore an excellent indicator for structure changes in the outer atmosphere with pulsation phase.

The matter is however complicated by the sensitivity of this VO band to the model $T_{\rm eff}$ as well. In the right-hand panel of Fig. 2 we show how its strength, relative to TiO, increases as $T_{\rm eff}$ is reduced in steps of 100 K from 2800 to 2200 K. When $\log(g) = -1.0$ it becomes noticeable around 2600 K, as the population density of its lower energy levels increases. However, for $\log(g) = -0.5$ (left-hand panel) it appears already around 2800 K. The reduced geometrical extension with higher $\log(g)$ raises the temperature structure over a wide range of low $T_{\rm eff}$ values. In other words, for these near-IR transitions we find that raising the gravity acceleration by a factor of three is equivalent to an increase of $T_{\rm eff}$ by ∼200 K in order to maintain similar temperature structures and electronic population densities in the formation region of this VO band. Since both atmospheric parameters are expected to vary with regular pulsation, this interdependence of the VO band strength can complicate a unique determination of ($T_{\rm eff}$, $\log(g)$ in a given variability phase. However, changes of $T_{\rm eff}$ have a different effect on the overall spectral energy distribution (SED), mainly by changing the optical and near-IR fluxes (i.e. following the Wien

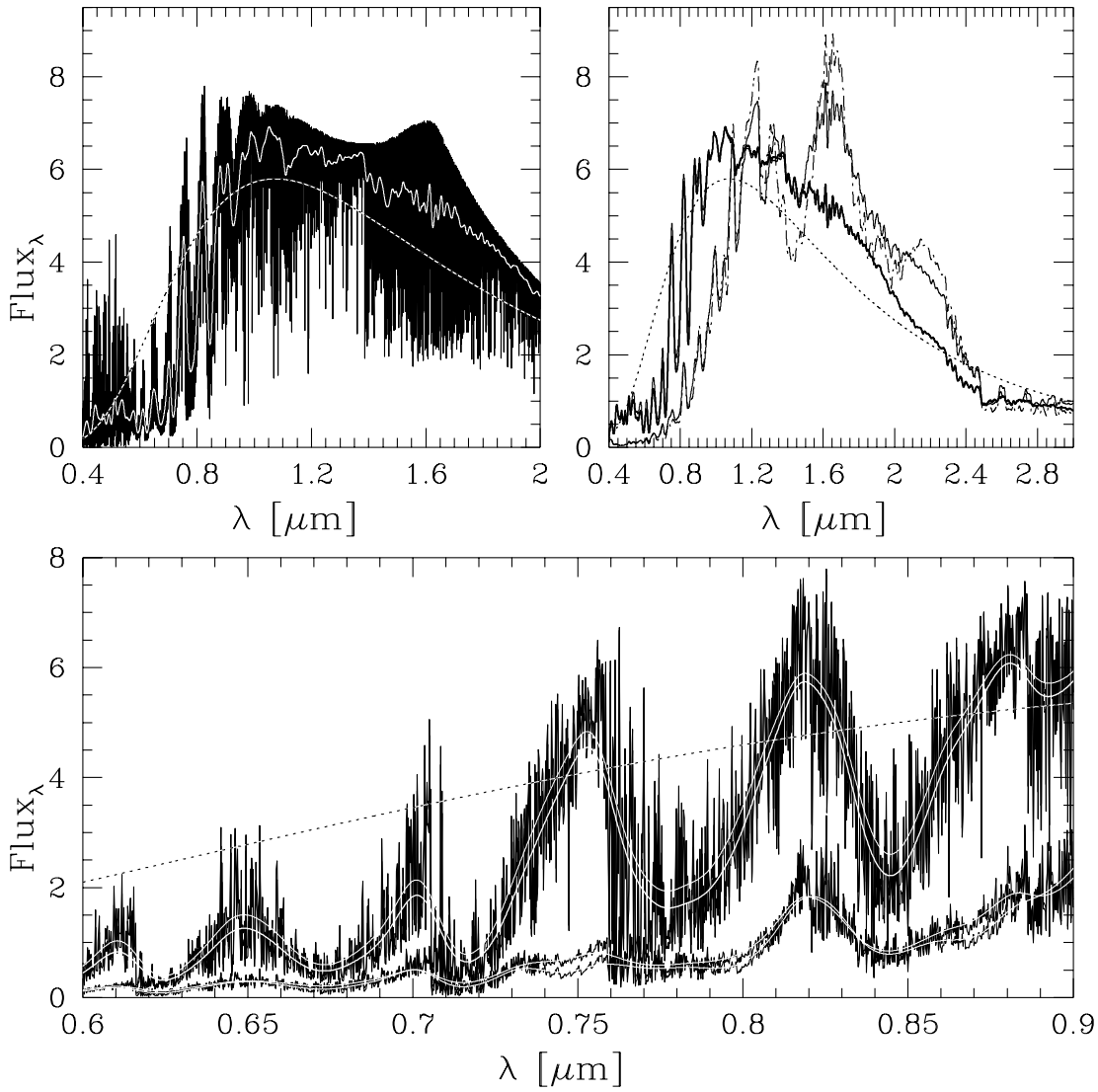

Figure 1. Upper left panel (a): a high-resolution model spectrum with $T_{\rm eff} = 2700$ K and $\log(g) = -1.0$ (black). Molecular absorption bands in these cool and extended atmospheres reduce the optical fluxes (white line) with respect to the corresponding blackbody continuum level (dotted line). Upper right panel (b): the mid-IR flux excess of the model spectra increases with higher $\log(g)$-values from -1.5 and -1.0 (bold line), -0.5 (thin line) to 0.0 (dash–dotted line). Lower panel (c): below 3000 K the relative intensity of the VO band at 0.75 μm increases with these values, which can be used to model observed spectra.

shift). We therefore model optical/near-IR spectra observed in various phases, together with coeval near-IR BB photometry and mid-IR spectrophotometry taken at similar phases (but not always within the same pulsation cycle).

2.2 Comparison with other giant models

We have compared the grid of PHOENIX giant models with some of the Uppsala models. The latter were computed with SOSMARCS, also in hydrostatic equilibrium (LTE) and spherical geometry (Plez, Brett & Nordlund 1992). These 11 models are offered in Fluks et al. (1994) and were used to represent the M0-M10 giant sequence with $T_{\rm eff}$ ranging from 2500 to 3900 K for solar composition. The stellar mass is $1.5\,{\rm M}_{\odot}$, where $\log(g)$ varies from -0.5 to 1.6. These high-resolution spectra show good correspondence in near-IR fluxes, and a similar strengthening of the VO band at 0.75 μm towards lower temperatures. Although Fluks et al. (1994) noted that the line strengths of the TiO γ- and γ'-systems have been rescaled in the Uppsala models following life-time measurements by Doverstål & Weijnitz (1992), we find good mutual agreement with the low-temperature PHOENIX models (i.e. $T_{\rm eff} = 2500$ K and $\log(g) = -0.5$ for M10) in the TiO band strengths, computed using the TiO opacities and molecular constants from Jørgensen (1994). In general the relative strength of these band-heads for both models compare better towards lower $T_{\rm eff}$, as they saturate below 3000 K. Note that Valenti, Piskunov & Johns-Krull (1998) found that the electronic oscillator strengths for the γ-system, applied here in the PHOENIX models, yield good agreement with the observed spectra of M dwarfs. A recent semi-empirical TiO model is discussed in Schwenke (1998) and extensive line lists have been computed and are provided via Kurucz (1999) website.

The PHOENIX models use opacities for the VO A–X and B–X bands computed via the Just Overlapping Line Approximation formulation (Brett 1990, and references therein), which were also used in the Uppsala models. Note however that Alvarez & Plez

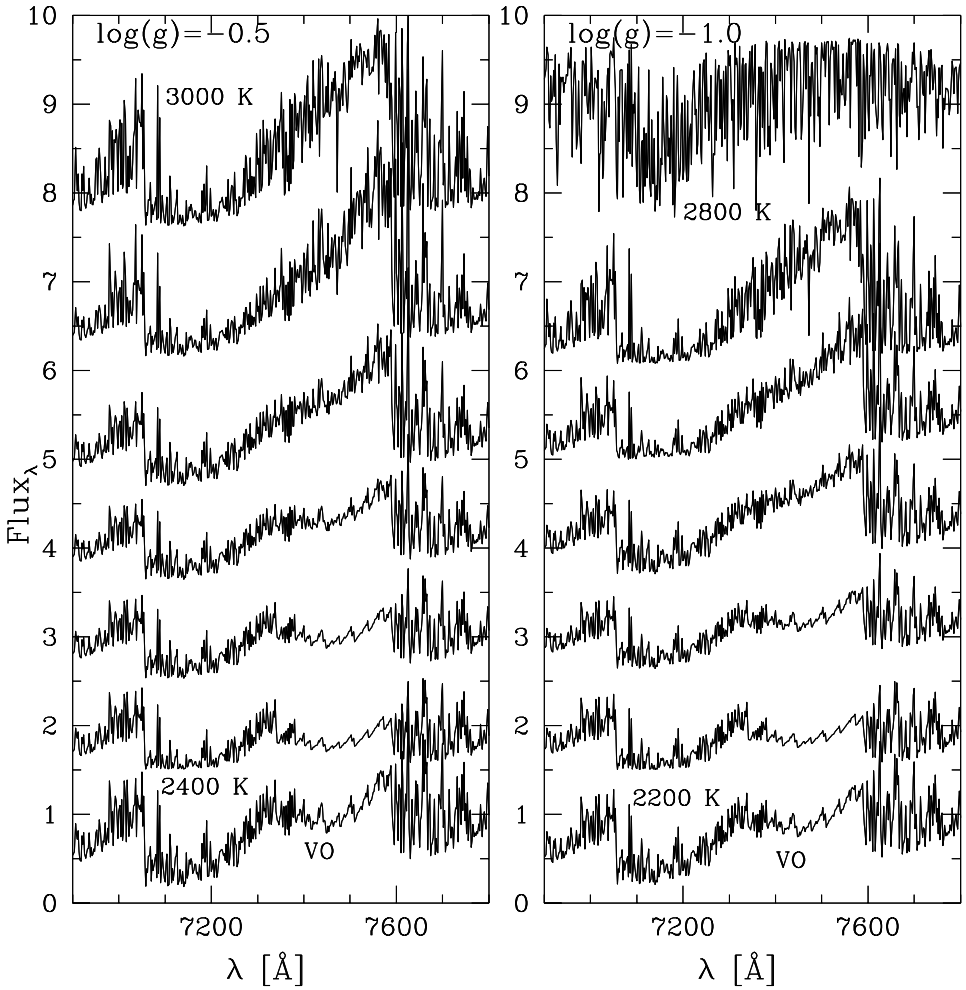

Figure 2. Right panel: at $\log(g) = -1.0$ the relative intensity of the VO band at 7450 Å strengthens with lower $T_{\rm eff}$ values and shows up around 2600 K. Left panel: for higher $\log(g) = -0.5$ it appears already for $T_{\rm eff} = 2800$ K as the atmospheric extension reduces, resulting in similar population densities in the formation region of this band. Its intensity is sensitive to both atmospheric model parameters.

(1998) recently compiled updated line lists of VO band systems, following new lifetime laboratory measurements by Hedgecock, Naulin & Costes (1995) and Karlsson et al. (1997). The latter would correspond to a rescaling of the VO B–X line strengths by a factor 0.28 relative to the JOLA approach. It indicates that the model parameters, which we derive below, based on the VO B–X band strength, could be off-set by as much as a few hundred degrees in $T_{\rm eff}$. However, we emphasize that we presently focus on finding ranges in the parameter changes with pulsation, rather than determining precise values for a given phase. The latter condition must be relaxed further owing to shortcomings in the present state of constructing low-gravity models. A discussion of possible NLTE effects on the strength of molecular bands is given in Plez et al. (1992). Such resonant scattering processes in tenuous outer layers would strengthen these bands rather than making them weaker. For the models we will apply, Allard et al. (1995) investigated departures from LTE but found only modest NLTE effects in the abundance of TiO.

2.3 Static and dynamic modelling

Scholz (1985) noted that the TiO and VO bands are formed in the upper (perhaps even non-photospheric) layers and provide a tool to measure the atmospheric extension. This follows directly from angular diameter measurements by Haniff, Scholz & Tuthill (1995), showing systematically larger photospheric diameters from fits to visibility curves taken in interference filters at 0.70 μm, when compared to near-continuum filters at 0.8–0.9 μm. Alvarez & Plez (1998) measured from 256 Miras a phase lag *between* various narrow-band colours in TiO and VO absorptions of the near-IR. They discussed whether such a shift may result from different formation depths caused by mechanical wave perturbations propagating through an extended atmosphere. Bessell et al. (1989) modelled the density structure for Miras between minimum and maximum light by injecting a shock wave each pulsation cycle. They showed that it can extend the atmosphere by a factor up to 2.5 between $\log(\tau_{\rm Ross}) = 0$ and -4. When comparing static and dynamic models they also found that synthetic narrow-band colours (for instance in the TiO γ-system $\lambda\lambda$7120–7450) would imply a temperature over 200 K cooler for the dynamic models. These differences are caused by changes in the effective atmospheric acceleration, which we will presently account for in our spectral fits, based however on hydrostatic models calculated for various $\log(g)$ values.

2.4 Circumstellar dust

The strong regularity of the light curve of these late-M Miras points to a radial oscillation of the continuum formation region. As for Cepheid pulsation it indicates that $T_{\rm eff}$ increases when the base of the atmosphere is collapsing. Its oscillation propagates delayed through an extended atmosphere on top, producing density waves that convey piston momentum upwards. At very small optical depths the kinetic temperature can periodically drop to below the dust nucleation limit of $\sim$1500 K causing species like TiO_2 or aluminium-oxides (like corundum) to condense out of the gas phase (Gail & Sedlmayer 1998). Note that Onaka, de Jong & Willems (1989) found indications for aluminium oxide particles from modelling *IRAS* LRS spectra of M-type giants. Such clusters serve as condensation seeds for SiO-bearing molecules, forming silicate grains while driven outward by radiation pressure. When sufficiently optically thin, the CDS produces a distinct emission feature at 9.7 μm of which the intensity is observed to vary with phase.

The dust medium can redistribute optical and near-IR fluxes to longer wavelengths determined by the shell thickness (or mass-loss rate). It is interesting that Plez et al. (1992) reported that the computed strengths of TiO bands are considerably too large with respect to observed bands in these wavelength regions. These model fits, which exclude the formation of dust, worsen with decreasing $T_{\rm eff}$. One may ascribe this to the poor quality of the present JOLA opacities (Bessell, Scholz & Wood 1996). However, it appears useful also to check the effect of the CDS on the near-IR spectra. We therefore presently model these spectra in conjunction with mid-IR dust emission observed at different phases.

3 MODELLING METHOD

3.1 Near-IR spectra

The observed spectra were recorded at Kitt Peak and the Dark Sky Observatory between 1996 February and 1997 January and were kindly provided to us by Dr M. Castelaz (private communication). First the raw spectra (in photon counts) were normalized as given in Castelaz & Luttermoser (1997, hereafter CL). The applied scaling factors (f) are listed in Table 1. Hence, from a visual inspection, clear differences in the relative intensity of the VO and TiO bands can already be discerned for different variability phases. A preliminary comparison with the models shows that the overall spectra are well represented for $T_{\rm eff}$ around 2500 K and solar composition. For $T_{\rm eff}$ above 3400 K the TiO bands become too faint, whereas for models with C/O $\geqslant$ 0.93 molecular bands due to C-compounds (like C_2) become too intense. Note that the TiO strength is also nearly independent of luminosity because the relation between spectral type and temperature (or colour) is at least approximately the same for dwarfs, giants and supergiants, despite their enormous luminosity differences (MacConnel, Wing & Costa 1992).

The variability phases assigned to the observed spectra are adopted from CL. These have been determined from visual brightness predictions by AAVSO (Mattei 1996) and have been used by us for an absolute flux calibration of the spectra (Table 1). An absolute scaling of the spectra also offers the advantage of approximating the bolometric flux changes from the model fits, as the latter can be integrated over the entire spectral range. To this end we have first corrected the V magnitude for interstellar reddening using the *Hipparcos* (ESA 1997) parallax for both stars. Its distance, together with the galactic co-ordinates, are used to compute $A_{\rm v}$ from the Galactic extinction law of Feast, Whitelock & Carter (1990). The corrected fluxes $V_{\rm F}$ are provided in Table 1. The normalized spectra for each phase are then convoluted with the V transmission function $T_{V_{\rm J}}(\lambda)$ in the Johnson system (Landolt-Börnstein 1982). This provides the scaling factor V_0 for the visual flux by which the normalized near-IR spectra $N(\lambda)$ have to be multiplied in order to calibrate them absolutely:

$$F(\lambda) = \frac{V_{\rm F}}{V_0} N(\lambda), \tag{1}$$

where

$$V_0 = \frac{\int_{V_{\rm J}} N(\lambda) T_{V_{\rm J}}(\lambda)\,{\rm d}\lambda}{\int_{V_{\rm J}} T_{V_{\rm J}}(\lambda)\,{\rm d}\lambda}. \tag{2}$$

Since the V passband ranges between $\lambda\lambda$4762 and 7407, whereas the observed near-IR spectra start only from λ6400, this filter has to be convoluted at the shorter wavelengths with the model spectrum that fits the observed spectrum best, in order to account for molecular absorptions that affect this visual band. The best model spectrum is selected from the available grid by means of a least-squares search method. We apply a simple logarithmic χ^2-estimator to each observed (and normalized) spectrum:

$$\chi_i^2 = \sum_{\lambda=\lambda_0}^{\lambda_1} [\log F^{\rm obs}(\lambda) - a_i \log F^{{\rm mod}(i)}(\lambda)]^2, \tag{3}$$

where a_i is varied in order to minimize χ^2 for every model spectrum i in the wavelength range between λ_0 and λ_1.

Table 1. Near-IR spectra modelled at different variability phases for *o* Cet and U Ori.

Star	Obs. date	JD 2 455 000+	V (mag)	Visible phase, ϕ	Dist. (*Hipp.*) (pc)	$V_{\rm F} \times 10^{14}$ (W cm^{-2} μm^{-1})	f $\times 10^4$	Model $T_{\rm eff}$ (K)	log(g) (cm s^{-2})	V_0 $\times 10^2$	$F_{\rm bol}^{\rm mod}$ $\times 10^6$ (erg s^{-1} cm^{-2})
o Cet	1996 Oct. 11	367.5	9.4	0.62	128	3.950	132.0	2400	−1.0	4.468	2.128
	1996 Dec. 14	431.5	5.9	0.81		14.47	0.011	2500	−1.0	9.335	6.758
U Ori	1996 Oct. 11	367.5	6.4	0.94	658	2.808	440.0	2700	−0.5	7.081	0.20
	1996 Dec. 14	431.5	6.7	0.12		0.2130	0.016	2700	−0.5	7.945	2.198
	1997 Jan. 26	474.5	7.9	0.24		0.07053	0.030	2400	−1.0	0.100	58.60
	1996 Mar. 2	144.5	12.6	0.32		0.009298	0.193	2400	−1.0	0.1286	821.0

$V_{\rm F}$ is the visual flux corrected for interstellar reddening.
f is the scaling factor to normalize the raw near-IR spectra.
V_0 is the conversion factor to calibrate them to an absolute flux scale.
$F_{\rm bol}^{\rm mod}$ is an estimate of the corresponding bolometric flux based on the model fits.

After the observed spectra have been absolutely calibrated, the model spectra are converted with their corresponding input blackbody spectrum to the absolute flux scale by means of a generated Planck function for the given $T_{\rm eff}$ and a value of the bolometric flux $F_{\rm bol}$. Thereafter, the search routine minimizes with Equation (3) the difference between the observed spectra and the model spectra in the absolute flux scale, where the fit variable a_i then provides the multiplication factor to estimate the bolometric flux of the selected model. We perform this iteration in a direct search over a grid of models with $2200\,{\rm K} \leqslant T_{\rm eff} \leqslant 3200\,{\rm K}$, for four values of $\log(g) = -1.5, -1.0, -0.5$ and 0.0. For each of these, the search routine selects the best $T_{\rm eff}$-value by matching the shape of the VO band and its intensity with respect of the TiO bands. The best model for every phase is then selected out of these four models by comparing their overall SEDs. Note that, in general, M-stars become redder when they become fainter in *V*, changing the $B-V$ index and other colours (Mendoza 1967; de Laverny et al. 1997).

3.2 Mid-IR spectro-photometry of dust emission

The mid-IR spectra were observed at UKIRT between 1994 August and 1997 August and kindly provided by Dr J. Monnier (private communication). The mean error in the absolute flux calibration is limited by ±10 per cent (see table 1 of Monnier et al. 1998) and remains below the observed intensity variations for the spectra we presently model. The 1995 August 20 spectrum of *o* Cet is modelled in conjunction with coeval near-IR BB photometry derived by us at Carlos Sanchez Telescope at Irzaña (Tenerife) on 1995 September 8 (Bagnulo 1996).

The spectrum of the central star at different phases is redistributed by frequency-dependent radiative transfer calculations through a spherically symmetric dust shell, whereby radiation momentum transfer drives the envelope expansion and determines its density structure and mass-loss rates. An application to the SED and variability of the carbon Mira R For can be found in Lobel, Doyle & Bagnulo (1999). For convenience we only provide the major improvements of this modelling method over previous work. The usual blackbody assumption for the stellar radiation field is abandoned, as atmospheric molecular and atomic line blanketing in these cool giants have strong effects on the shape and fluxes of the output spectrum. These opacity sources affect the 'synthetic' BB-photometry we compute from the reprocessed spectra by convolution with the transmission function in each passband. The dust shell parameters are determined by means of a least-squares search on the observed BB-photometry in conjunction with a best fit to the intensity and shape of coeval observations of the silicate feature.

Our radiative transport calculations consider the stationary outflow of dust that drags the ambient gas along. The resulting density and temperature structures, starting from the dust condensation point, are monotonically decreasing functions of distance in the dust shell. The bolometric flux is conserved within 95 per cent. We apply a grain size power-law distribution of the form $n(a) \propto a^{-q}$, having sharp boundaries at $a_{\rm min} \leqslant a \leqslant a_{\rm max}$. The absorption and scattering efficiencies are evaluated via the Mie theory for grains treated as homogeneous spheres. The optical constants for olivine silicate are taken from Dorschner et al. (1995), which allows us to reproduce the mid-IR spectra better than the optical constants of 'astronomical silicate' derived by Draine & Lee (1984) and Laor & Draine (1993), traditionally adopted for reproducing the SEDs of oxygen-rich dust-obscured objects.

Ivezić & Elitzur (1995) determined the shell conditions of *o* Cet, R Leo, χ Cyg and other oxygen-rich Miras with optically thin dust envelopes and computed gas mass-loss rates of typically $2\text{–}4 \times 10^{-7}\,{\rm M}_{\odot}\,{\rm y}^{-1}$. From the SED modelling of 27 oxygen-rich stars, Le Sidaner & Le Bertre (1996) demonstrated a strong correlation of the shell optical depth and mass-loss rates to the (K-12 μm) colour. Bagnulo (1996) modelled coeval SEDs and UKIRT mid-IR dust emission spectra of eight optically visible oxygen-rich stars. These fits overestimate the optical BB photometry as input blackbodies were assumed. This was also found by Le Sidaner & Le Bertre (1993) for the Mira IRC −30023 with $\tau_{10} \sim 0.08\text{–}0.15$. From the SED modelling they found temperatures at the inner dust condensation radius in the range 750–950 K. A study of variability revealed that the temperature curves in the dust shell vary parallel between minimum and maximum phase with $T_{\rm eff}$ changes of the central star by 200 K. We will presently test if such changes in the conditions of the circumstellar environment can model the shape changes observed in the silicate emission with phase.

4 RESULTS

4.1 *o* Ceti (Mira)

4.1.1 Atmospheric model parameters and pulsation

Two near-IR spectra, taken at $\phi = 0.62$ and $\phi = 0.81$ (phase zero refers to maximum visual brightness), were modelled with the technique outlined in Section 3.1. For the spectrum taken at $\phi = 0.62$, the method retains two models with ($T_{\rm eff}$, $\log(g)$-parameters equal to (2400, −1.5) and (2400, −1). For the spectrum at $\phi = 0.81$ the search method selects four possible models: (2500, −1.5), (2500, −1), (2700, −0.5) and (2900,0.0). Fig. 3(c) shows the χ^2 versus $T_{\rm eff}$ curves for various values of $\log(g)$ at phase $\phi = 0.81$. The straightforward application of our least-squares technique does not permit us to determine the stellar parameters uniquely based on near-IR spectra at these two pulsation phases. For this purpose, other (independent) constraints have to be considered.

The model with (2900,0.0) (at $\phi = 0.81$) can be ruled out since Mahler, Wasatonic & Guinan (1997) recorded the visual light curve during this pulsation period and found that the visual magnitudes at both phases $\phi = 0.62$ and 0.81 are close to the minimum (which occurs around $\phi = 0.7$). Only at phases beyond $\phi = 0.85$ does *V* rise steeply to 2.5 mag, viz. near $\phi = 1.0\text{–}1.1$ (1997 February). Furthermore, an extrapolation of the period–gravity relation for radial pulsation by Fernie (1995) shows that $\log(g) = 0.0$ is too high for stars that, like *o* Cet, have a pulsation period >300 d. In fact, a mean value of −0.6 is usually adopted for Miras. This suggests that the candidate models with (2500, −1.5) (at $\phi = 0.81$) and (2400, −1.5) (at $\phi = 0.62$) should not be favoured to represent these phases. Therefore, at phase 0.62 we adopt the model with (2400, −1.0), whereas for $\phi = 0.81$ we are left with two possibilities: (2500, −1.0) or (2700, −0.5). In order to discriminate between these two models, we discuss the effect of a 0.5 dex change of the atmospheric acceleration.

When assuming that the changes of the effective acceleration in the outer layers are mainly caused by the pulsation motions at the base of the atmosphere, an increase of $\log(g)$ by 0.5 dex implies a decrease of the stellar radius (or the continuum formation layers)

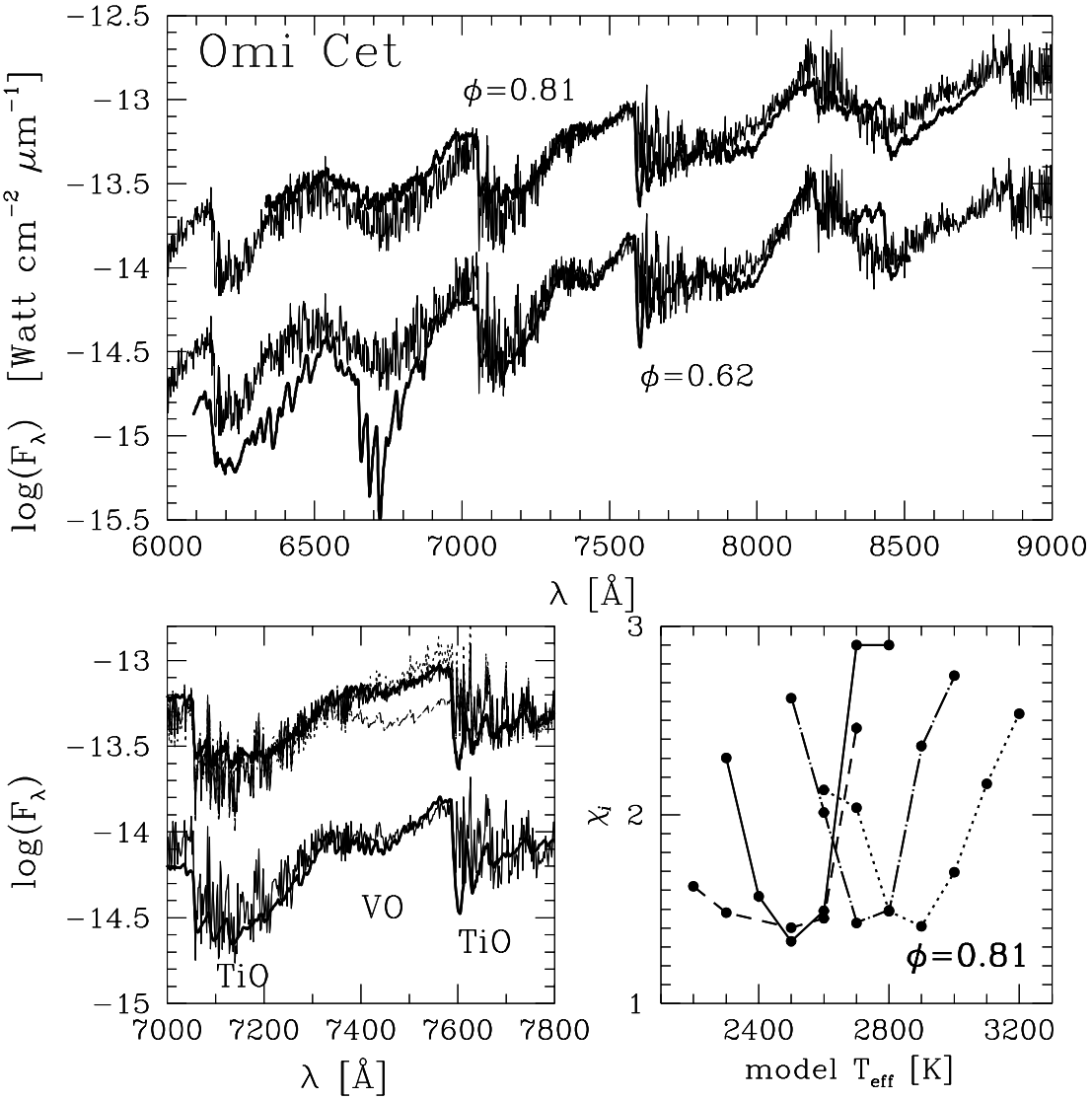

Figure 3. Upper panel (a): a best fit to the near-IR spectrum of Miras observed at $\phi = 0.62$ and $\phi = 0.81$ (bold solid lines) is derived for $T_{\rm eff} = 2400$ and 2500 K, respectively (thin solid lines) with $\log(g) = -1.0$ (or -1.5). Lower left panel (b): in 64 d (at $\phi = 0.81$) the relative intensity of the VO band at 7450 Å has become weaker, indicating an increase of $T_{\rm eff}$ by 100 K. Models for $T_{\rm eff} = 2600$ K, which do not fit the VO band at $\phi = 0.81$, are shown for $\log(g) = -1$ (thin dotted line) and -0.5 (thin dashed line). Lower right panel (c): best model parameters are determined from a χ^2-minimization search between the observed spectra and the model grid, for four values of $\log(g) = -1.5$ (dashed line), -1.0 (solid), -0.5 (dash–dotted) and 0.0 (dotted) (see text).

by a factor $\sqrt{3}$. For an estimated mean stellar radius of $\sim 500\,R_\odot$ this is equivalent to a displacement of $212\,R_\odot$ over a period of 64 d, which requires a mean velocity of $\sim 27\,{\rm km\,s^{-1}}$ during the collapse. This value appears incompatible with amplitudes of optical absorption line radial velocity curves observed in Miras. These variations in general do not exceed $10\,{\rm km\,s^{-1}}$ (Barbier et al. 1988) and remain below $5\,{\rm km\,s^{-1}}$ for *o* Cet. Note for example that Ferlet & Gillet (1984) observed the infall of matter in Mira (o Cet) with supersonic velocities from near-IR inverse P-Cygni profiles just after the luminosity maximum.

However, if a change of 0.5 dex is mainly caused by large-scale mass motions in the upper atmosphere, an integration over 64 d for an acceleration of $\log(g) = -1$ and -0.5 gives a displacement of $\sim 23\,R_\odot$ and $\sim 70\,R_\odot$. Such a radial displacement of the entire upper atmosphere would result in a luminosity increase (from $\phi = 0.62$ to $\phi = 0.81$) by a factor $(2700/2400)^4 \cdot (430/500)^2 = 1.18$, which appears consistent with the observations by Mahler et al. (1997) of $L_* \sim 6000\,L_\odot$ at $\phi = 0.6$ and $7700\,L_\odot$ at $\phi = 0.8$. However, in this case we compute mean downflow velocities of 6 and $17\,{\rm km\,s^{-1}}$ for $\log(g) = -1.0$ and -0.5, respectively, which renders the model with (2500, -1.0) more consistent with the observed amplitude of its radial velocity curve.

The model with (2500, -1.0) is also supported by the calibrations of Mahler et al. (1997), based on narrow-band Wing photometry (Wing 1992). They estimate a change of $T_{\rm eff}$ from 2400 to 2500 K between these two phases. The minimum at 2500 K in the χ^2-curve for $\log(g) = -1.0$ in Fig. 3(c) is not significantly lower than the minimum at 2700 K for $\log(g) = -0.5$, but the arguments given above favour the former. Note however that the higher χ^2-values for models with other $T_{\rm eff}$ are significant and these do not fit the shape of the VO band, as is shown in Fig. 3(b) for $T_{\rm eff} = 2600$ K.

4.1.2 *Circumstellar dust shell parameters*

We have used the model adopted for $\phi = 0.81$, with $(T_{\rm eff}, \log(g) = (2500, -1.0)$, as input to the DUSTY code to calculate the overall SED after redistributing the stellar radiation through an optically thin dust shell with $\tau_{9.7} = 0.025$ (further details on the determination of the dust shell parameters are given below).

At optical wavelengths, flux differences between the input model and the output spectrum are very small; thus, the redistributed flux also nearly fits the near-IR spectrum observed in 1996 December ($\phi = 0.81$). We have also compared the model SED with a set of coeval observations obtained in 1995 August, i.e. *JHKL′* BB-photometry, and a UKIRT mid-IR spectrum (see Fig. 4). The latter epoch corresponds to phase $\phi = 0.37$, which is nearly symmetric around the minimum of the light curve to phase $\phi = 0.81$, suggesting that the stellar temperature and $\log(g)$ of these two phases are similar. This comparison should be regarded with some caution, since Mira (o Cet) is a binary. The spectrum of Mira B has separately been resolved with *HST* (Karovska et al. 1997), displaying a maximum in the SED around 0.36 μm, which could result from a compact companion of about $T_{\rm eff} = 12\,000$ K. Mira B is however about two magnitudes fainter than the giant near the minimum phase ($V_{\rm min} \sim 9.4$ mag in 1995 December). Its effect on the near-IR fluxes and long-ward should therefore be negligible in the present modelling.

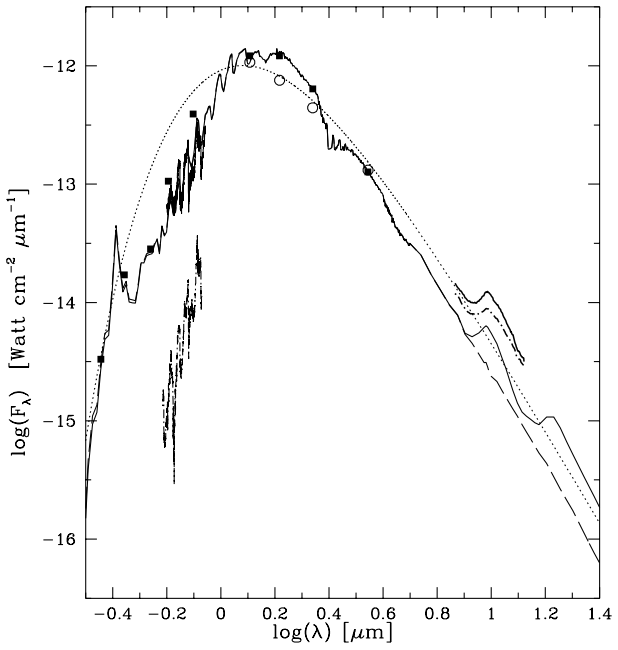

Figure 4. A fit to the mid-IR BB photometry of Mira (o Cet) observed at $\phi = 0.37$ in 1995 September (open circles) is derived by computing synthetic BB fluxes (solid boxes) from the spectrum (thin solid line), which is reprocessed through the CDS with $\tau_{9.7} = 0.025$ for the input model with $T_{\rm eff} = 2500$ K and $\log(g) = -1.0$ of $\phi = 0.81$ (dashed line). The redistributed flux at 9.7 μm underestimates the flux observed in the coeval silicate feature (bold solid line). The corresponding blackbody (dotted line) matches the flux of its blue wing, but strongly overestimates the absolute flux observed in the near-IR spectrum of 1996 December ($\phi = 0.81$). For comparison, we show also the flux of the silicate feature observed near the minimum (phase $\phi = 0.68$, 1995 December, bold dash–dotted line) and the near-IR spectrum obtained at $\phi = 0.62$ (1996 October, thin dash–dotted line).

The synthetic BB fluxes (solid boxes in Fig. 4) nearly match the observed IR photometry (open circles), fixing the bolometric flux at 2.22×10^{-5} erg s^{-1} cm^{-2}. Note that the blackbody curve (dotted line), corresponding to the same effective temperature of the input model, would predict a much higher flux at shorter wavelengths, although it seems to be in better agreement with the observed IR photometry, and with the absolute flux of the mid-IR spectrum. Indeed, the input model with $\log(g) = -1.0$ (dashed line of Fig. 4) gives a background flux that is too small to fit the observed intensity at 9.7 μm. This discrepancy would disappear if we adopted an input model with slightly higher $\log(g) = -0.5$, but this would lead to an overestimate of the observed IR BB photometry.

It should be noted that the background fluxes *cannot* sufficiently be increased by changing the parameters of the dust shell, which is very optically thin (see Fig. 5). It is therefore probable that this discrepancy results from an inaccurate prediction in the flux levels of the input spectrum at longer wavelengths. For a detailed fit to the observed mid-IR spectrum, we have therefore scaled the stellar input flux up by $\Delta \log(F_\lambda) = 0.2$.

The value of the optical depth of the CDS is well constrained by the shape of the mid-IR dust emission feature. We find that it sensibly sharpens by raising the value of its optical depth (Fig. 5a). For the grain size we find that a best fit is obtained with a size distribution $n(a) \propto a^{-3.5}$, with $0.01\ \mu{\rm m} \leqslant a \leqslant 0.15\ \mu{\rm m}$ (Fig. 5b). However, our radiative transport calculations reveal that the temperature $T_{\rm c}$ at the inner shell radius $R_{\rm c}$ and the geometric shell thickness d are harder to constrain. We find a valid range for $T_{\rm c}$ between 600 and 1200 K (Fig. 5c), and d between 10 to $10\,000\,R_{\rm c}$ (Fig. 5d). The latter indeterminacy can be understood as there is only a little dust near $R_{\rm c}$, and the dust density reduces quickly with r^{-2} at greater distances. We also compute that T_c below 600 K produces a flux in the silicate feature that is too weak and the flux at 18 μm would strongly over-estimate the *IRAS* LRS flux.

In Fig. 5 we have also plotted the *IRAS* LRS spectrum (dots). The slope of the red wing of the latter is slightly steeper and the computed profiles fit somewhat better than to the UKIRT spectrum of 1995. These shape differences possibly result from long-term changes in the distribution of dust around Mira (o Cet). We checked that such strong changes of this emission slope cannot be reproduced by changing the dust density distribution in our spherical symmetric radiative transfer computations, for instance by applying multiple dust shells (a discussion of changes in dust emission features observed on time scales significantly longer than the stellar pulsation period is given in Monnier, Geballe & Danchi 1999).

In the next section we discuss how the shape variability of the observed silicate feature provides information on the changing conditions of the CDS.

4.1.3 *Variable dust emission*

Mahler et al. (1997) measured the total amplitude of the visual light curve in 1996–1997 of $\Delta V \simeq 6.5$ mag. These amplitudes level off towards longer wavelengths where $\Delta J \simeq 1.3$ mag, $\Delta H \simeq 1.2$ mag, $\Delta K \simeq 0.9$ mag and $\Delta L \simeq 0.66$ mag as was observed by Catchpole et al. (1979) in 1975–1978. Lopez et al. (1997) estimated the amplitude changes in the *N*-passband (with effective wavelength around 10.2 μm) to be below 1 magnitude (or $\Delta \log(F_\lambda) \leqslant 0.4$) after 1990. Since the dust shell of the Mira is very optically thin below 10 μm, the decreasing trend in the amplitude of light curves at shorter wavelengths (which is also

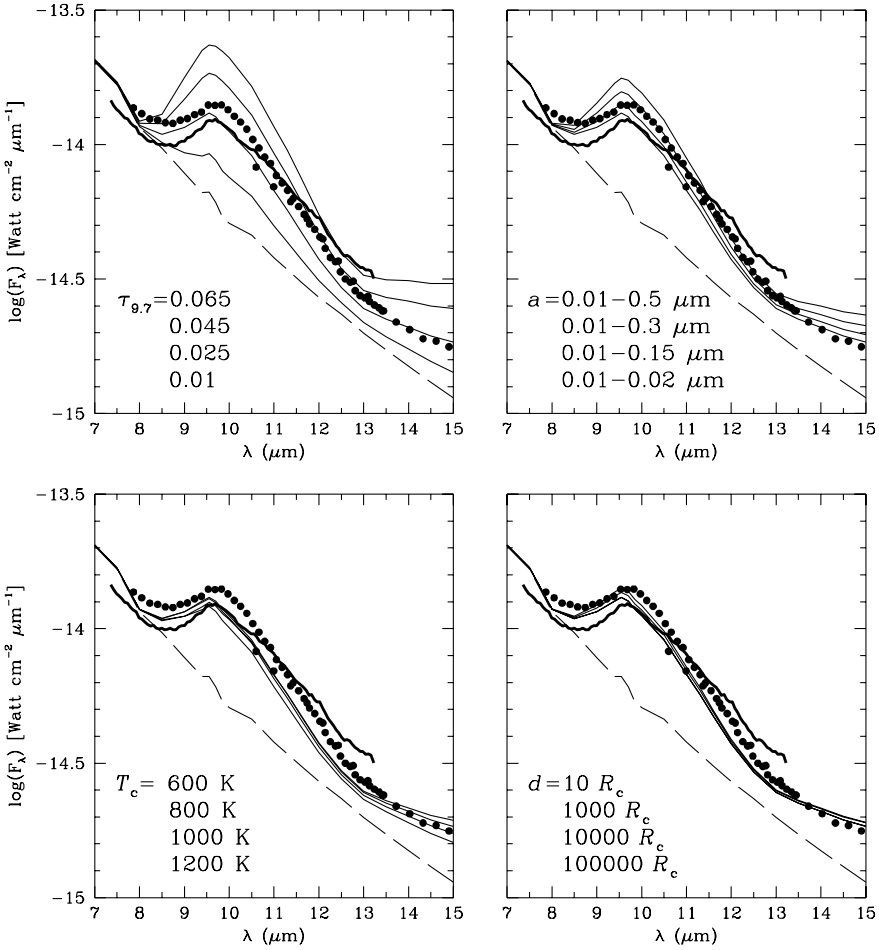

Figure 5. The four panels show the intensity of the silicate feature computed with radiative transfer through the CDS composed of olivine grains, for different values of the shell optical depth $\tau_{9.7}$, the grain size distribution of $n(a) \propto a^{-3.5}$ between minimum and maximum grain sizes, the temperature T_c at the inner dust radius R_c and the geometrical shell thickness d (thin solid lines). A best fit to the emission feature observed for Mira (o Cet) in $\phi = 0.37$ (bold solid line) is derived for $\tau_{9.7} = 0.025$ and $a \leqslant 0.15\,\mu$m. Since the shell is very optically thin, the bolometric flux of the selected input model spectrum (dashed line) can be scaled at 8.5 μm to match the observed flux in this phase. The *IRAS* LRS spectrum is shown by the dots.

observed for other oxygen-rich Miras; e.g. Le Bertre 1993) is mainly due to a combined effect of luminosity and temperature variations with phase. This indicates that the lag of the near-IR maxima by ∼0.1 of a period behind the visual maxima observed by Lockwood & Wing (1971) and by Maran et al. (1977) at 2.7 μm cannot be explained by a modulation of the near-IR fluxes due to the CDS. It is therefore likely that this lag rather originates in the stellar atmosphere proper, possibly due to its large extension and by the mechanisms that convey heat and momentum upward.

In Fig. 6 we show the best fit to the silicate feature observed at phases $\phi = 0.37$, 0.68 and 0.29. This latter phase is near to the visual maximum of 1994 August, and the shape of the dust emission profile and its intensity (with respect to the background flux) is best fitted with an input model with $T_{\rm eff} = 3000$ K and $\log(g) = -0.5$. Note that the blue shoulder of the silicate feature is too weak computed for $T_{\rm eff} = 2900$ K and it becomes too intense for 3100 K. In this phase when the feature is sharpest we detect differences of 100 K from the emergent dust emission spectra. Scaling the redistributed spectrum for 3000 K to the blue flank of the emission hump corresponds to a bolometric flux of $F^{\rm bol}_{\rm max} = 2.40 \times 10^{-5}\,{\rm erg\,s^{-1}\,cm^{-2}}$. For the phase near minimum light ($\phi = 0.68$) of 1995 December with $T_{\rm eff} = 2400$ K we find $F^{\rm bol}_{\rm min} = 1.95 \times 10^{-5}\,{\rm erg\,s^{-1}\,cm^{-2}}$, yielding a total light reduction of $\sim 18 \pm 2$ per cent. The error is derived by flux integrating emergent SEDs computed for $\Delta T_{\rm eff} = 100$ K. In the same phase this produces small differences in the mid-IR and IR fluxes (which contribute most to $F_{\rm bol}$), but the integration results in minor differences after scaling them to the flux observed in the blue wing of the mid-IR dust feature.

For a radial oscillation of the atmosphere we thus find a change of the mean stellar radius with $R_{\rm min}/R_{\rm max} = \sqrt{1.954/2.404}(3000^2/2400^2) = 1.408$, or an increase by about 41 per cent near minimum light. Note that Tuthill, Haniff & Baldwin (1995) found strong indications for real changes in the extent of the stellar atmosphere from large variations in Mira's visibility function of 1993, whereas changes in the asymmetric source flux remained moderate. They reported variations of the apparent size as large as ∼15 per cent over time-scales of a few months from angular diameter measurements at 0.71 μm, but which are usually much smaller in the pseudo-continuum bands at 0.833 and 0.902 μm.

The flux changes of $\Delta \log(F_\lambda) \simeq 0.2$ around 8.5 μm in the blue flank of the silicate feature (see Fig. 6a) can therefore chiefly be ascribed to the luminosity and temperature (i.e. radius) changes of the central star between the minimum and maximum phases.

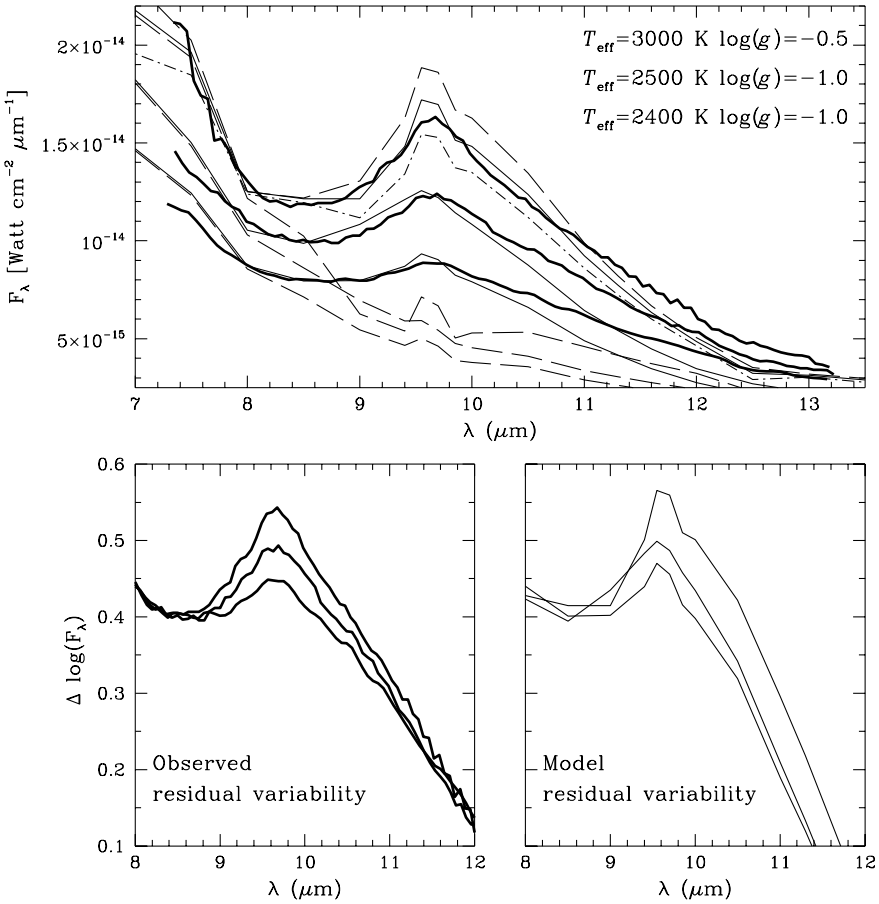

Figure 6. Upper panel (a): best fits (thin solid lines) to the silicate emission of Mira (o Cet) observed in the minimum phase ($\phi = 0.68$, 1995 December 2), $\phi = 0.37$ (1995 August 20) and near maximum light $\phi = 0.29$ (1994 August 26) (bold solid lines). The corresponding input spectra are shown by the dashed lines for $T_{\rm eff} = 2400$, 2500 and 3000 K, respectively. The observed variations in absolute flux result from changes in the bolometric flux of the stellar input spectrum with phase. In the maximum phase the feature shape is best fitted for 3000 K, but it is too weak for 2900 K (dash–dotted line) and too intense for 3100 K (dashed line). Lower left panel (b): the luminosity changes are removed by matching the observed flux levels in different phases at 8.5 μm in the logarithmic scale. Lower right panel (c): the residual changes of its shape result from small variations in the dust acceleration with $T_{\rm eff}$ or the flux mean optical depth of the CDS. These best fits are computed without changing the grain composition, $n(a)$, $T_{\rm c}$ or d with phase.

In Fig. 6(b) we have plotted the silicate feature of Mira (o Cet), observed in three phases, in the logarithmic flux scale. Shifting the spectra to an equal flux level near 8.5 μm allows us to remove the effect of the bolometric flux changes. The remaining differences of shape and width (or contrast with respect to the same background level) with phase can then entirely be ascribed to changes of emissitivity in the CDS proper. This 'residual' variability displays a clear contrast enhancement near maximum light, rendering it somewhat broader and sharper by $\Delta \log(F_\lambda) \simeq 0.1$ between the minimum and maximum phases.

In Fig. 6(c) we plot the model residual variability derived from our best fits with radiative transfer through the CDS. The residual changes of the width and intensity are best modelled for $T_{\rm eff}$ changes from 2400 and 2500 K to 3000 K. In our calculations we keep fixed the dust grain parameters to $T_{\rm c} = 800$ K, $d = 10\,000\,R_{\rm c}$, $q = 3.5$, $a_{\rm min} = 0.01$ μm and $a_{\rm max} = 0.15$ μm. As $T_{\rm eff}$ rises near maximum light, the SED hardens by increasing the flux of the incident radiation field at shorter wavelengths. The transfer of radiation momentum to the dust, forming near $R_{\rm c}$, becomes therefore more efficient. In Fig. 7 we show that it cyclically increases the acceleration of dust in this region, whereby the terminal velocity of the dust outflow ($v_\infty^{\rm dust} \simeq 48\,{\rm km\,s^{-1}}$) varies by $\sim 5\,{\rm km\,s^{-1}}$ between minimum and maximum phase. This has a profound effect on the flux mean opacity $\tau_{\rm F}$ of the CDS which varies between 0.939×10^{-2} and 1.037×10^{-2} to 1.141×10^{-2} over the three phases. These changes in flux density of the dust outflow cause the variability of dust emission flux observed around 9.7 μm. They result without having to invoke changes in the dust properties themselves. This is also supported by the difference between the observed and the input spectra (normalized to 8.5 μm), which are almost equal up to a scaling factor. We find that the shape variability of the silicate feature is a dynamical mean-opacity effect in the CDS, caused by variable dust acceleration by the stellar SED in cases where the CDS is optically very thin.

As the dust density is very small, the drag force of the dust results in very low terminal gas outflow velocities of about $4.5\,{\rm km\,s^{-1}}$. From a Gaussian fit to the CO(J = 1–0) millimetre emission line, Knapp & Morris (1985) measured the terminal outflow velocity of the gas envelope to be $6\,{\rm km\,s^{-1}}$. The small changes in dust density and terminal gas velocity in the CDS (with $\Delta v_\infty^{\rm gas} \leqslant 1\,{\rm km\,s^{-1}}$, indicating that the CO linewidth stays practically invariant with phase), result in changes of the gas mass-loss rate from $2.79 \times 10^{-7}\,{\rm M_\odot\,yr^{-1}}$ and $2.99 \times 10^{-7}\,{\rm M_\odot\,yr^{-1}}$ to

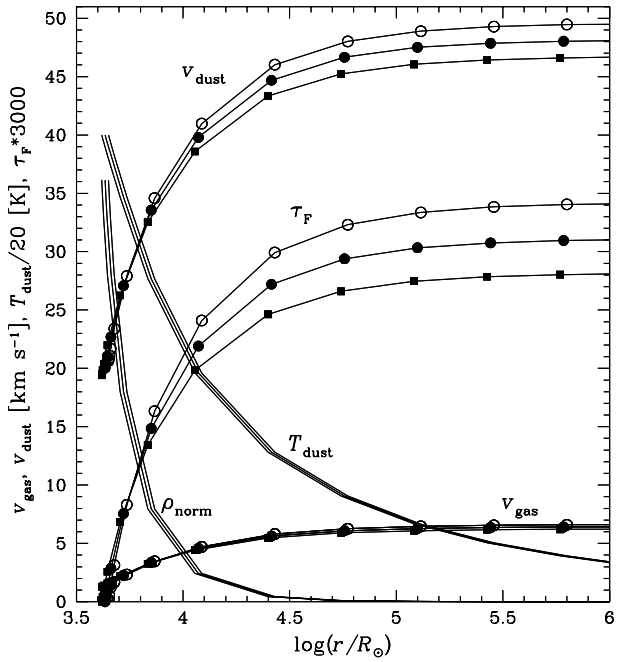

Figure 7. The terminal dust velocity V_{dust} assumed by radiation pressure on the CDS of Mira (o Cet) accelerates by $\sim$5 km s^{-1} from minimum (boxed line) to maximum phase (open circles). An increase of T_{eff} by 600 K enhances the radiative driving of the CDS and increases its flux mean optical depth τ_F by $\sim$0.002. The gas outflow velocity V_{gas} stays almost invariable and assumes much smaller (almost sub-sonic) terminal velocities as the dust density and its drag forces are very small. The normalized dust density assumes an r^{-2} distribution for a steady-state outflow, showing little variation of its gradient with phase near $R_c \sim 6R_*$. We have adopted $T_c = 800$ K and compute that the dust temperature drops to $\sim$90 K at $100R_c$ and to $\sim$20 K at $10^4 R_c$, following a nearly fixed gradient.

3.19×10^{-7} M$_\odot$ yr^{-1} in the maximum phase, where we have assumed a dust grain bulk density of 3 g cm^{-3} and a canonical gas-to-dust mass ratio of 200. The latter values may be too small, since Knapp & Morris (1985) compute 6.5×10^{-7} M$_\odot$ yr^{-1} for an optically thin envelope. On the other hand our model values are in better agreement with the K I and Na I scattering measurements of 1.0×10^{-7} M$_\odot$ yr^{-1} by Mauron & Caux (1992) or 2.0×10^{-7} M$_\odot$ yr^{-1} derived by Skinner & Whitmore (1988). Although Mira's binarity invalidates an assumption of spherically symmetric mass-loss, most importantly our calculations show appreciable changes of $\dot{M}$ by $\sim 0.4 \times 10^{-7}$ M$_\odot$ yr^{-1} per cycle ($\sim$10 per cent), even if we keep the stellar luminosity fixed to $L_* = 10^4$ L$_\odot$ in every phase.

We compute that R_c (i.e. $(T_{eff}/T_c)^2 \sim 6 R_*$) increases from 2.89×10^{14} cm and 3.0×10^{14} cm to 3.11×10^{14} cm in the maximum phase, which corresponds to an increase of R_c from $\sim$4150 R$_\odot$ by $\Delta R_c \sim 300$ R$_\odot$ when the stellar atmosphere collapses. The increased radiative driving produces higher mass-loss rates and thus amplified radiation from shells where the 9.7-μm dust emission emerges.

4.2 U Orionis (HIP 28041)

The light curve of the Mira U Orionis (M6-M9.5e) displays an asymmetry (the slope of the rising branch being slightly steeper than the descending branch) and an amplitude very similar to that of *o* Cet. Its *Hipparcos* reference period (ESA 1997) is 367 d. In Fig. 8 we show best fits to the near-IR spectra derived from the search method outlined in Section 3.1. The spectra of phases $\phi =$ 0.94 and 0.12 (Table 1) were obtained around the visual maximum of 1996 November and are best fitted by model spectra with $T_{eff} = 2700$ K and $\log(g) = -0.5$. The spectrum of 1996 March 2 ($\phi = 0.32$) was obtained before the preceding visual minimum of 1996 August (see, for example, the AAVSO light curve on the Internet). For this phase and for the spectrum of $\phi = 0.24$ (1997 January) our search method selects $T_{eff} = 2400$ K and $\log(g) = -1.0$. The selected synthetic spectra confirm our finding for *o* Cet that lower T_{eff} values correspond to a smaller effective acceleration in the stellar atmosphere.

Next the selected model spectra are redistributed through a model of the CDS to match the shape and intensity of the silicate feature observed at corresponding variability phases. The four mid-infrared spectra we model in Fig. 9(a) were however derived one pulsation cycle earlier. The shape of the silicate feature observed at $\phi = 0.3$ (of 1995 March) is best fitted when redistributing the selected model spectrum with $T_{eff} = 2400$ K ($\phi = 0.32$ of Fig. 8) through a model of the dust envelope, composed of olivine grains, with $\tau_{9.7} = 0.045$, $T_c = 800$ K, $d = 10\,000 R_c$, $q = 3.5$, $a_{min} = 0.01$ μm and $a_{max} = 0.15$ μm. Note for instance that Bauer & Stencel (1994) adopt $T_c = 970$ K for U Ori and 840 K for *o* Cet in order to model 60-μm emission from silicate grains. Although very optically thin, we find that the optical depth of the dust shell at 9.7 μm around U Ori is about twice as large as for *o* Cet, resulting in a stronger contrast of the silicate emission feature under otherwise similar conditions. For the phases when the residual intensity was stronger at $\phi = 0.13$ (1995 January) and $\phi = 0.01$ (1995 December) we utilize the selected input spectrum of 2700 K ($\phi = 0.12$ of Fig. 8) and 2900 K ($\phi = 0.94$), respectively. Note that the input spectrum with 2700 K derived from the fits to the near-IR spectrum in Fig. 8 proved slightly too cool (by approximately 200 K) to match the constrast of the silicate feature at $\phi = 0.01$ and to reproduce its observed residual variability, shown in Fig. 9(b). We think that this small difference in the model temperature can be ascribed to the visual maximum, which was actually about half a magnitude brighter (when the silicate feature was observed) than the following visual maximum when the near-IR spectrum was obtained.

We find that our radiative transfer calculations through the CDS strongly match the observed residual variability of the dust emission feature of U Ori by varying the T_{eff} of the input SED by $\sim$500 K. As for *o* Cet, the longwave shoulder of the computed feature is somewhat too weak to fit the observations. We were unable to remove these minor flux differences by varying the conditions in the dust shell or by changing the input SED. We therefore speculate that it may result from contributions in the actual (unknown) dust composition, which differs from pure olivine grains. Note also that the blue shoulder of the feature appears somewhat steeper than in *o* Cet (Fig. 6a), particularly near maximum intensity. This steepness could be modelled by lowering the input model $\log(g)$ to -1.0 and T_{eff} to 2700 K for the maximum phase (dash–dotted line). This removes the broad absorption band around 9 μm from the input spectrum (dashed lines), which can lower the emergent intensity of the blue emission flank of the silicate feature. Nevertheless, these adapted model parameters appear incompatible with the intensity of the VO band observed around this phase. In Fig. 8 we observe that the band is clearly visible near 7450 Å, whereas it is absent in the

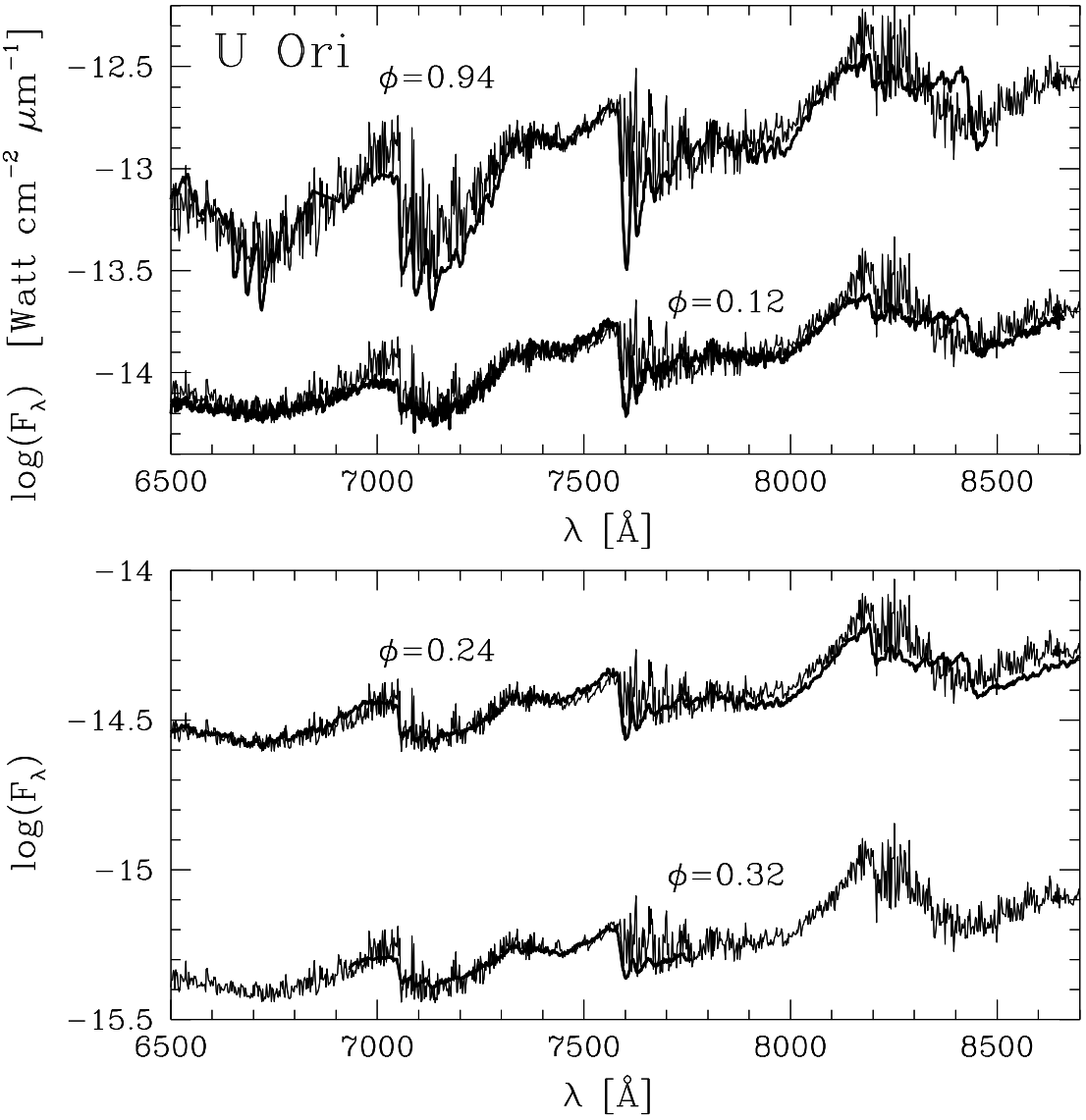

Figure 8. Best fits (thin solid lines) to the near-IR spectra of the Mira variable U Ori observed in four different phases (bold solid lines). Upper panel: the relative intensity of the VO band for two phases $\phi = 0.94$ and 0.12 near the visual maximum correspond to $T_{\rm eff} = 2700$ K and $\log(g) = -0.5$. Lower panel: the spectra for $\phi = 0.24$ and 0.32 are best fitted for $T_{\rm eff} = 2400$ K and $\log(g) = -1.0$.

model spectra with $\log(g) = -1.0$ and $T_{\rm eff} = 2700$ K (see Fig. 2). This observation indicates that further improvements for the detailed modelling of the shape of variable dust emission in Miras will require input SEDs that are computed and selected for a refined mesh with grid points smaller than $\Delta\log(g) = 0.5$ and $\Delta T_{\rm eff} = 100$ K, and that are redistributed through the CDS with very high dispersion ($\leqslant$100 Å) up to mid-IR. Such modelling work still exceeds the memory and time-numerical capacity of modern computational facilities.

In Fig. 10 we show the dust acceleration for the three phases modelled in Fig. 9. We derive terminal outflow velocities for the gas component of 7 km s^{-1}. Bowers & Johnston (1988) proposed an approximately spherical gas distribution expanding at a constant radial velocity of 8 ± 1 km s^{-1}, based on the 1665 MHz OH maser emission line. They also mentioned that no indications for binarity of U Ori have been found so far. These OH maser observations with VLA provided mass-loss rate estimates of 8.0×10^{-8} M$_\odot$ yr^{-1} (Bowers, Johnston & de Vegt 1989).

We compute that the outflow velocity of the dust component is limited by $\sim$43 km s^{-1} and varies by only 3 to 4 km s^{-1} during the variability cycle. When assuming a dust grain bulk density of 3 g cm^{-3} and a gas-to-dust mass ratio of 200 (as for *o* Cet) we compute a change of the gas mass-loss rate from 4.42×10^{-7} M$_\odot$ yr^{-1} to 4.59×10^{-7}M$_\odot$ yr^{-1} and 4.9×10^{-7} M$_\odot$ yr^{-1}. For fixed $L_* = 10^4$ L$_\odot$ we thus compute changes of the mass-loss rate by $\sim 0.5 \times 10^{-7}$ M$_\odot$ yr^{-1} within the pulsation cycle, caused by changes of $\sim$500 K in the temperature of the incident radiation field. The flux-averaged total optical depth $\tau_{\rm F}$ in the CDS changes from 1.687×10^{-2} to 1.784×10^{-2} and 1.958×10^{-2} over the three phases, which results in an enhanced dust emission flux observed at 9.7 μm. We compute that the increased radiation pressure on the dust shell changes $R_{\rm c}$ from 2.90×10^{14} cm (4167 R$_\odot$) to 2.97×10^{14} cm and 3.08×10^{14} cm, corresponding to an increase of $\Delta R_{\rm c} \sim 260$ R$_\odot$, similar to that for *o* Cet.

The CO(J = 1–0) line emission was not detected in the study of Knapp & Morris (1985), but Young, Phillips & Knapp (1993)

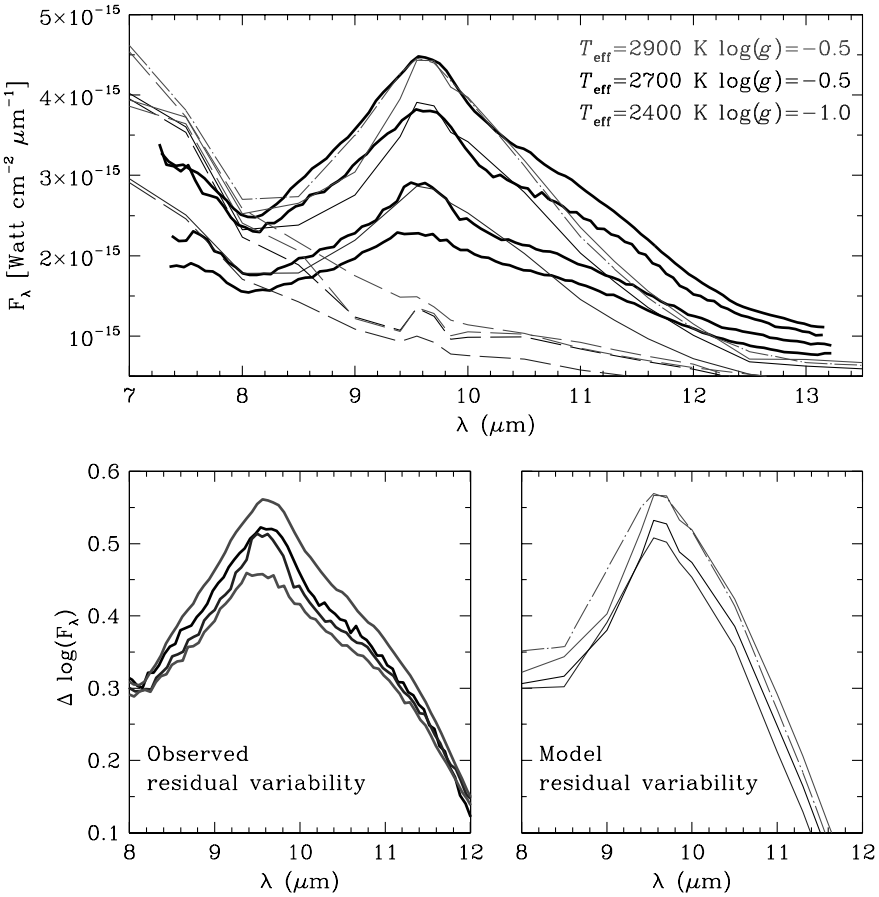

Figure 9. Upper panel (a): best fits (thin solid lines) to the silicate emission of U Ori observed near the minimum phase ($\phi = 0.73$, 1995 August 20), $\phi = 0.3$ (1995 March 17), $\phi = 0.13$ (1995 January 14) and near maximum light $\phi = 0.01$ (1995 December 2) (bold solid lines). The input spectra are shown by the dashed lines for $T_{\rm eff} = 2400$ K ($\phi = 0.3$), 2700 K ($\phi = 0.13$) and 2900 K ($\phi = 0.01$). The thin dash–dotted line improves the fit to the blue shoulder of the emission hump at $\phi = 0.01$ by lowering the input log(g) from -0.5 to -1.0 (see text). Lower left panel (b): the effect of luminosity change with phase is removed from the feature by matching the observed flux levels at 8 μm in the logarithmic scale. Lower right panel (c): the residual changes in its shape result from small changes in the dust acceleration with phase. Note the sharper contrast of the feature compared to *o* Cet due to the larger optical depth of the CDS of U Ori at 9.7 μm.

tabulated an expansion velocity of 7.5 km s^{-1}, which was derived from an unpublished CO(J = 3–2) spectrum. Hence they compute a mass-loss rate of 2.7×10^{-7} M$_\odot$ yr^{-1} for a distance of 240 pc with the radiative transfer program of Morris (1980). This could indicate that the gas-to-dust mass ratio of 200, used in our modelling of U Ori, is a factor of ∼2 too large. However Gehrz & Woolf (1971) estimated a mass-loss rate of 1.2×10^{-6} M$_\odot$ yr^{-1} from mid-IR spectral characteristics. Note further that Rowan-Robinson & Harris (1983) computed 2.5×10^{-7} M$_\odot$ yr^{-1}, and Danchi et al. (1994) derived 2.9×10^{-7} M$_\odot$ yr^{-1} (for a distance of 250 pc) from dust modelling work.

As for *o* Cet, the radiation driven dust density assumes an r^{-2} distribution. The gradients of both dust density and temperature show only small changes during the variability cycle, whereas the dust flow velocity slightly accelerates near $R_{\rm c}$ in the phase of higher $T_{\rm eff}$. Changes of the dust temperature at $R_{\rm c}$ are unable to model the observed shape changes of the silicate feature. Shortward of this emission, the dust shell of U Ori is very optically thin and we find no appreciable effect on the emergent optical and near-IR fluxes. We therefore conjecture that its decreasing magnitude range with longer wavelengths (see Catchpole et al. 1979), which is generally observed for Miras with optically thin dust shells, results from complex pulsation dynamics in an extended atmosphere, rather than by radiative transfer through the dusty environments of these evolved stars.

5 CONCLUSIONS

(*i*) We show that changes of the stellar model parameters $T_{\rm eff}$ and effective acceleration log(g) of late-M Miras can be derived from a detailed modelling of the shape and intensity of the VO band at 7450 Å observed with good dispersion at different variability phases. This modelling requires a high-resolution grid of spectral models for oxygen-rich giants computed for these parameters. In the case of Mira (o Cet) we find a change of $T_{\rm eff}$ from 2400±100 K at minimum light to about 3000 K near the maximum phase. Our modelling measures changes of $T_{\rm eff}$ as small as 100 K between two phases observed around the visual minimum, where a value of log(g) = −1.5 or −1.0 (±0.5) is derived from these hydrostatic models.

(*ii*) The detailed model spectra determined at different phases are redistributed through a spherically symmetric model of the circumstellar dust shell. These detailed radiative transfer calculations are carried out in order to fit the shape and intensity of silicate dust emission observed at corresponding variability phases. We find that Mira has a very optically thin dust envelope

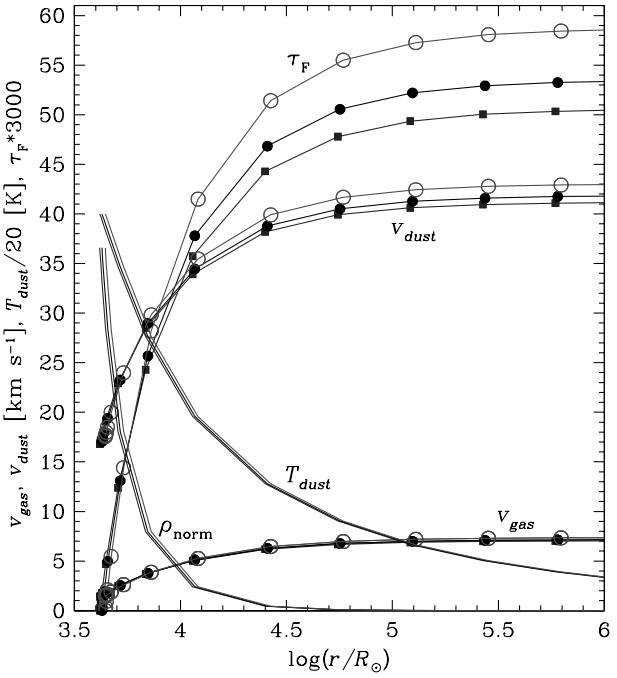

Figure 10. As the radiation pressure on the CDS of U Ori changes with phase, the dust terminal velocity $V_{\rm dust}$ varies by $\sim$3 km s^{-1} when $T_{\rm eff}$ changes by 500 K between $\phi = 0.3$ (boxed line) and $\phi = 0.01$ (open circles). The slightly increased mass-loss rate increases the flux mean optical depth $\tau_{\rm F}$ of the CDS and the silicate emission flux at 9.7 μm.

with $\tau_{9.7} = 0.025$, with a grain size distribution of the form $n(a) \propto a^{-3.5}$, having grain sizes smaller than $\sim$0.15 μm. We show that the sharpening of the dust emission near the visual maximum results from an increase of $T_{\rm eff}$ by about 600 K, which increases the dust acceleration and dust flux in the 9.7-μm emission region. This produces appreciable variations of the radiation-driven mass-loss rate by 0.4×10^{-7} M$_\odot$ yr^{-1} ($\sim$10 per cent) and the related flux mean optical depth of the CDS by $\sim$0.002. The dust envelope of U Ori is only slightly optically thicker with $\tau_{9.7} = 0.045$, displaying changes of $\dot{M}$ of 0.5×10^{-7} M$_\odot$ yr^{-1} when $T_{\rm eff}$ changes by 500 K. Best fits are derived with optical properties measured for an olivine grain composition. We find however that the shape changes observed with phase in the dust emission can be modelled without invoking changes of this composition, the grain size fractions, its temperature at the inner shell radius or the geometrical extension of the envelope. It is a dynamical effect in the CDS whereby the terminal dust outflow velocity varies by only $\sim$5 km s^{-1}, leaving its gas density- and temperature-distribution practically unchanged with phase, caused by its small optical thickness.

(*iii*) Our modelling shows that the small optical thicknesses of the dust envelopes of the latest-M Miras have negligible effect on the SED shortward of 10 μm. Therefore the intensity of molecular bands in these wavelength regions remains practically unaffected, and amplitude differences or phase lags observed between optical and near-IR light curves have to be ascribed to the photospheric dynamics proper. For the same reason, luminosity or $T_{\rm eff}$ changes will directly influence the intensity of the silicate emission with phase. The differences in variability of shape and intensity observed between these Miras therefore results from slight differences in their shell mean optical thickness and of the luminosity amplitude. These shape changes enhance as the shell mean optical depth increases and its amplitude variations grow with larger luminosity ranges.

ACKNOWLEDGMENTS

We thank the referee Dr Z. Ivezić for thoroughly commenting on an early version of this paper. The authors are grateful to Dr M. Castelaz for providing us with near-IR spectra of Miras in different phases and to Dr J. Monnier for providing UKIRT spectra of variable dust emission in these objects. We thank Dr R. Kurucz for stimulating discussions on this modelling work. This work was in part carried out under PPARC Grant L21259. AL acknowledges financial support by the Smithsonian Astrophysical Observatory. SB has been supported by the Austrian *Fonds zur Förderung der Wissenschaftlichen Forschung*, Project P12101-AST. Research at Armagh Observatory is grant-aided by the Department of Education for Northern Ireland, while partial support is provided in terms of both software and hardware by the STARLINK Project which is funded by the UK PPARC. The UKIRT is operated by the Joint Astronomy Centre on behalf of PPARC.

REFERENCES

Allard F., Hauschildt P. H., 1995, ApJ, 445, 433
Allard F., Scholz M., Wehrse R., 1992, Rev. Mex. Astron. Astrof., 23, 203
Allard F., Lawlor T., Alexander D. R., Hauschildt P. H., 1995, BAAS, 187, 10311
Alvarez R., Plez B., 1998, A&A, 330, 1109
Bagnulo S., 1996, PhD thesis, Queen's Univ. Belfast, p. 116
Barbier M., Mayor M., Mennessier M. O., Petit H., 1988, A&AS, 72, 463
Bauer W. H., Stencel R. E., 1994, AJ, 6, 107, 2233
Bessell M. S., Brett J. M., Scholz M., Wood P. R., 1989, A&A, 213, 209
Bessell M. S., Scholz M., Wood P. R., 1996, A&A, 307, 481
Bowers P. F., Johnston K. J., 1988, ApJ, 330, 339
Bowers P. F., Johnston K. J., de Vegt C., 1989, ApJ, 340, 479
Brett J. M., 1990, A&A, 231, 440
Castelaz M., Luttermoser D. G., 1997, AJ, 114, 1584 (CL)
Catchpole R. M., Robertson B. S. C., Lloyd Evans T. H. H., Feast M. W., Glass I. S., Carter B. S., 1979, SAAO Circulars Vol. 1, 61
Creech-Eakman M. J., Stencel R. E., Williams W. J., Klebe D. I., 1997, ApJ, 477, 825
Danchi W. C., Bester M., Degiacomi G., Greenhill J., Townew C. H., 1994, AJ, 107, 1469
de Laverny P., Geoffray H., Jorda L., Kopp M., 1997, A&AS, 122, 415
Dorschner J., Begemann B., Henning T., Jager C., Mutschke H., 1995, A&A, 300, 503
Doverstål M., Weijnitz P., 1992, Mol. Phys., 75, 1375
Draine B. T., Lee H. M., 1984, ApJ, 285, 89
ESA, 1997, The *Hipparcos* Catalogue, ESA Sp-1200
Feast M. W., Whitelock P. A., Carter B. S., 1990, MNRAS, 247, 227
Ferlet R., Gillet D., 1984, A&A, 133, L1
Fernie J. D., 1995, AJ, 110, 2361
Fluks M. A., Plez B., Thé P. S., de Winter D., Westerlund B. E., Steenman H. C., 1994, A&AS, 105, 311
Gail H.-P., Sedlmayer E., 1998, in Faraday Discussions No. 109, Chemistry and Physics of Molecules and Grains in Space. The Royal Society of Chemistry, London, p. 303
Gehrz R. D., Woolf N. J., 1971, ApJ, 165, 285
Haniff C. A., Scholz M., Tuthill P. G., 1995, MNRAS, 276, 640
Hedgecock I. M., Naulin C., Costes M., 1995, A&A, 304, 667
Ivezić Z., Elitzur M., 1995, ApJ, 445, 415
Ivezić Z., Nenkova M., Elitzur M., 1996, User Manual for DUSTY, available on the Internet: http://www.pa.uky.edu/moshe/dusty/
Jørgensen U. G., 1994, A&A, 284, 179

Karlsson L., Lindgren B., Lundevall C., Sassenberg U., 1997, J. Mol. Spectrosc., 181, 274
Karovska M., Hack W., Raymond J., Guinan E., 1997, ApJ, 482, L175
Knapp G. R., Morris M., 1985, ApJ, 292, 640
Kurucz R. L., 1999, TiO line list from Schwenke (1998). Kurucz CD-ROM No. 24 and on the Internet: http://cfaku5.harvard.edu/molecules/TiO/
Landolt-Börnstein 1982, in Schaifers K., Voigt H. H., eds, Numerical Data and Functional Relationships in Science and Technology, Stars and Star Clusters, Vol. 2b. Springer, New York, p. 71
Laor A., Draine B. T., 1993, ApJ, 402, 441
Le Bertre T., 1993, A&AS, 97, 729
Le Sidaner P., Le Bertre T., 1993, A&A, 278, 167
Le Sidaner P., Le Bertre T., 1996, A&A, 314, 896
Little-Marenin I. R., Stencel R. E., Staley S. B., 1996, ApJ, 467, 806
Lobel A., Doyle J. G., Bagnulo S., 1999, A&A, 343, 466
Lockwood G. W., Wing R. F., 1971, ApJ, 169, 63
Lopez B. et al., 1997, ApJ, 488, 807
MacConnell D. J., Wing R. F., Costa E., 1992, AJ, 104, 2
Mahler T. A., Wasatonic R., Guinan E., 1997, IBVS, 4500
Maran S. P. et al., 1977, Infrared Phys., 17, 565
Mattei J. A., 1996, Predicted Dates of Maxima and Minima of Long Period Variables for 1996. AAVSO Bulletin 59
Mauron N., Caux E., 1992, A&A, 265, 711
Mendoza E. E., 1967, AJ, 72, 311
Miller F. D., 1956, AJ, 61, 186
Monnier J. D., Geballe T. R., Danchi W. C., 1998, ApJ, 502, 833
Monnier J. D., Geballe T. R., Danchi W. C., 1999, ApJ, 521, 261
Morris M., 1980, ApJ, 236, 823
Onaka T., de Jong T., Willems F. J., 1989, A&A, 218, 169
Plez B., 1992, A&AS, 94, 527
Plez B., Brett J. M., Nordlund Å., 1992, A&A, 256, 551
Rowan-Robinson M., Harris S., 1983, MNRAS, 202, 767
Scholz M., 1985, A&A, 145, 251
Schwenke D. W., 1998, Proc. Faraday Soc., Discussion No. 109, 321,
Skinner C., Whitmore B., 1988, MNRAS, 234, 79
Tuthill P. G., Haniff C. A., Baldwin J. E., 1995, MNRAS, 277, 1541
Valenti J. A., Piskunov N., Johns-Krull C. M., 1998, ApJ, 498, 851
Wing R. F., 1992, JAAVSO, 21, 42
Young K., Phillips T. G., Knapp G. R., 1993, ApJ, 409, 725

This paper has been typeset from a TEX/LATEX file prepared by the author.